To appear in Mechanics of Materials (2008)

Thermo-mechanical aspects of adiabatic shear failure of AM50 and Ti6Al4V alloys

D. Rittel[1] and Z. G. Wang
Faculty of Mechanical Engineering
Technion
32000 Haifa, Israel

[1] *Corresponding author:* merittel@technion.ac.il

ABSTRACT

The thermo-mechanical aspects of adiabatic shear band (ASB) formation are studied for two commercial alloys: Mg AM50 and Ti6Al4V. Tests are carried out on shear compression specimens (SCS). The evolution of the temperature in the deforming gauge section is monitored in real time, using an array of high speed infrared detectors synchronized with a Kolsky apparatus (split Hopkinson pressure bar). The evolution of the gage temperature is found to comprise 3 basic stages, in agreement with Marchand and Duffy's simultaneous observations of mechanical data and gauge deformation patterns (1988). The onset and full formation stages of ASB are identified by combining the collected thermal and mechanical data. Full development of the ASB is identified as the point at which the measured and calculated temperature curves intersect and diverge thereon. At that stage, the homogeneous strain assumption used in calculating the maximum temperature rise is no longer valid.

Keywords: Mg AM50, Ti6Al4V, adiabatic shear band, IR detectors, Hopkinson bar

Thermo-mechanical aspects of adiabatic shear failure of AM50 and Ti6Al4V alloys

1. INTRODUCTION

Adiabatic shear banding (subsequently referred to as ASB) is a coupled thermo-mechanical phenomenon leading to the catastrophic failure of ductile materials subjected to dynamic (high strain rate) loading. The ASB is a narrow band (surface) of intense strain localization, in which extremely rapid and local heating effects can bring the local temperature close to the melting point of the shocked material. Many materials have been investigated during the last 4 decades, using various experimental methods, in order to identify the conditions and relevant material properties leading to the initiation and growth of ASB (Bai and Dodd, 1992).

One of the key experimental issues relates to monitoring the evolution of the temperature in the dynamically deforming gauge section of a specimen, until final failure. The most popular method consists of infrared detection of the surface radiation emitted from the deforming specimen (Walley, et al., 2000). Duffy and co-workers were among the first to use a focused, imaging system of IR detectors for dynamic shear experiments (Duffy and Chi, 1992; Hartley, et al., 1987). Infrared detectors were also applied to dynamic fracture studies, to monitor temperature changes at crack-tips (Zehnder and Rosakis, 1991). Additional refinement to the method was brought by Zehnder et al. (2000), who characterized the temperature fields inside propagating shear bands, using a specially developed high-speed thermal camera with full field imaging capabilities. Zhou et al. (Zhou, et al., 1996a; 1996b) investigated the initiation and propagation of shear bands by subjecting pre-notched plates (C-300 steel and Ti6Al4V) to asymmetric impact loading (dynamic mode-II). In addition to the IR detectors, Mason et al. used high-speed photography and the method of coherent gradient sensing (CGS) to record the full deformation field around an adiabatic shear band emanating from a pre-crack tip in C-300 steel loaded dynamically in mode II (1994).

Emphasizing constitutive modeling, Macdougall and Harding (1999) obtained shear stress-strain curves for thin-walled tubular specimens of Ti6Al4V alloy for a wide range of strain rates, up to $1000/s$. These authors used an infrared radiometer to measure the

rise in specimen surface temperature during the high strain rate tests, and derived the material constants used in the Zerilli-Armstrong constitutive relation.

A different, yet related issue, is that of the amount of mechanical *energy* converted into heat during adiabatic deformation, which was first investigated by Farren and Taylor (1925) and by Taylor and Quinney (1934). These authors investigated the conversion of mechanical energy into heat, through a ratio, generally referred to as the β factor. In a subsequent work carried out on a glassy polymer, Rittel (1999) defined 2 factors: the first, which was noted by β_{int}, is precisely Taylor and Quinney's (1934) factor β. The second factor, noted β_{diff}, appears in the coupled heat equation (Boley and Weiner, 1960). This factor is defined as the ratio of the thermal to mechanical *power*. The expressions for the 2 factors are given by Rittel (1999):

$$\beta_{diff}(\varepsilon,\dot{\varepsilon}) = \frac{\rho C_p \dot{T}}{\dot{W}_p} \qquad (1)$$

$$\beta_{int}(\varepsilon,\dot{\varepsilon}) = \beta = \frac{\rho C_p \Delta T}{W_p} \qquad (2)$$

Where T is the temperature, W_p is the plastic work, ρ is the density, Cp is the specific heat, and dotted quantities indicate time-derivatives. Consequently, eqn (1) describes a ratio of mechanical powers, whereas equation (2) describes a ratio of mechanical works. Note that eqn. (2) can be used to calculate ΔT, knowing β, or β if ΔT is measured.

Kapoor and Nemat-Nasser (1998) measured thermal signals by using a 4-channel IR detector to determine the fraction of plastic work converted to heat (β_{int}). They reported that close to 100% of the work done during high strain rate deformation is converted to heat. On the other hand, Hodowany et al. (2000) reported results pertaining to 2024-T3 aluminum alloy and α titanium showing that β_{int} is both strain and strain-rate dependent. Similar trends were reported by Rittel (1999) for polycarbonate. His results showed a definite dependence of the two β factors on the strain and strain rate. Whereas the overall ratio (β_{int}) of the converted energy remains inferior to 1 as expected, the rate ratio (β_{diff}) may reach values superior to 1 at the higher strain rates.

As of today, there is an impressive number of experimental observations of adiabatic shear bands. The emphasis has been mostly put on the microstructure of the shear band (post-mortem), with a scarcity of real-time measurements of the temperature rise and distribution. The seminal contribution of Marchand and Duffy (1988) was the first attempt to identify the various stages leading to ASB formation and its subsequent evolution. Three stages were identified in the degree of strain homogeneity, based on visual recording of a fiducial grid pattern. The recorded images were correlated with the recorded stress-strain curves. No attempt was made to correlate the mechanical and the thermal results that were independently recorded. These results were mainly focused on the maximum temperature rise inside a shear band, which is one of the most impressive characteristics of this failure mechanism.

Simultaneous assessments of stress-strain-temperature in the shear band are still quite rare, except for Macdougall and Harding's recent work (1999). However, for these torsion tests, the temperature and the stress are usually reported as a function of time,. While the time scale can always be converted into a strain for a given strain-rate, it would nevertheless be very instructive to obtain *simultaneous* stress and temperature versus strain relations. Such measurements are also crucial for proper physical understanding and modeling of thermo-mechanical effects related to adiabatic shear band formation, in which the large temperature rise is assumed to be the key factor (Zener and Hollomon, 1944). Yet, the evolution of an ASB from its onset until final failure cannot be unequivocally identified from the sole dynamic flow curve of a material. Open questions remain to be answered, such as what is the role of the pre-localization (homogeneous) temperature rise, and how does an ASB form. Namely is ASB a brutal bifurcation process, or more the rapid, yet smooth, loss of strain homogeneity as described by Marchand and Duffy (1988)?

Consequently, the goal of this study is a simultaneous determination of the dynamic mechanical and thermal response of Mg AM50 and Ti6Al4V alloys (Rittel, et al., 2006), in order to obtain a better physical understanding of the ASB formation process. The present experiments concentrate on dominant shear deformation, using the shear compression specimen, SCS (Rittel, et al., 2002) for which the temperature is monitored using an infrared detector array.

1. EXPERIMENT

Materials and specimens

Mg AM50 and Ti6Al4V were selected as the experimental materials in this study, as they are prone to failure by ASB mechanism (Rittel, et al., 2006). The first material is a magnesium-aluminum alloy AM50 (ASTM B94), supplied as cylindrical bars. Microstructural characterization is an Al-Mg solid solution (matrix) which contains elongated (typically 1μm long) β phase ($Mg_{17}Al_{12}$) and Al_8Mn_5 precipitates. The second material is a commercial annealed titanium alloy (Ti6Al4V). The typical microstructures of un-deformed materials are shown in Figure 1.

The composition and selected mechanical-physical properties of these two materials are listed in Tables I and II, respectively.

Mechanical testing

As mentioned above, shear compression specimens (SCS) (Rittel, et al., 2002) were tested using the compression split Hopkinson bar. This specimen consists of a pair of diametrically opposed grooves that make a 45º angle with the longitudinal axis of a cylinder. The main advantage of this specimen is that it can be used indifferently for quasi-static and dynamic (high-rate) tests, with the same data reduction technique. In a typical split Hopkinson test, the interfacial loads and displacements are recorded and reduced into stress and strain data respectively. The principle of the current tests is identical, except that because of the special specimen geometry, one must map the measured loads and displacements into equivalent stress and strain in the gauge section comprised between the grooves (Rittel, et al., 2002). This process requires preliminary numerical simulations, but the final validation comes from a comparison of the stress-strain characteristics of the investigated material, using both SCS and cylindrical specimens. By contrast with cylindrical or torsion specimens, the deformed gauge of the SCS is and remains planar throughout the test, thereby minimizing variations of focusing distance of the IR setup. It also appears that the change of surface condition of the specimen is not as significant as that of cylindrical specimens. This relates to the fact

that IR emission from a surface is affected by the surface condition (emissivity). This point was not thoroughly investigated here as the overall strain levels at failure remained rather modest in the present tests. It is also important to note that, similar to a regular split Hopkinson test, the equilibrium of the specimen is ascertained for each test by comparing the interfacial measured loads. The typical strain rate for the experiments reported in this work is $\dot{\varepsilon} \approx 3000\,\mathrm{s}^{-1}$.

Thermo-mechanical testing systems

Figure 2 is a schematic illustration of the experimental apparatus used in this study. There are two main parts: one is the standard Kolsky apparatus (SHPB), made of 17-4 PH steel bars with a diameter of 19.05mm; the rest is the thermal signal measurement system, including a 1:1 magnification optical system (double Schwartzchild, Figure 3), an eight channel IR detector, ((liquid N2 cooled MCT array, Fermionics PV 12-45-8), a signal pre-amplifier (Fermionics PVA 500-5) and a digital signal acquisition system (PXI computer with two NI PXI-6113 S series sampling cards). As shown in Figure 4, each element of the detector is a $45 \times 45\mu\mathrm{m}$ square, and the center-to-center pitch between two neighboring elements is $50\mu\mathrm{m}$, and the whole array covers a distance of $395\mu\mathrm{m}$. The IR detectors are high-speed infrared detectors with a rise time of approximately 15ns.

The system allows a simultaneous characterization of the thermal and the mechanical processes associated with ASB formation. The output signal generated by the strain gauge on the incident bar of the SHB is used to trigger the digital oscilloscope that record the signals from the high-speed IR detectors. It should be noted that IR monitoring is used to determine the specimen's superficial temperature.

The optical system (schematically represented in Figure 3) was observed to have a relatively large depth of field. In any case, before each and every experiment, the specimen, optical system and detectors are all aligned so that radiation could be optimally collected from a well defined point on the gauge section.

The infrared detector collects the IR radiation and outputs a proportional voltage. It should be mentioned that for metallic specimens of the dimensions (shown in figure 5) used in this work, the gauge's surface temperature matches closely the core temperature for transient measurements, according to the analysis of Rabin and Rittel (2000).

The linear array of the IR detectors is horizontal, and to minimize the effect of the movement of specimen on the thermal signals during the dynamic experiment, the detectors need to be pointed to the central part of the deformed gauge of the SCS specimen (Figure 5). A preliminary finite element model of the dynamically loaded SCS showed that the Y axis motion of the specimen does not exceed 0.7 mm in a typical test (Dorogoy, 2005). Consequently, central focusing maintains the gauge section in the field of view of the detector.

It should be understood that, in each experiment, the optical system "looked" at the central part of the gauge section. There is no possibility to focus on an adiabatic shear band when the latter does not emanate from a pre-existing defect, so that its origin and trajectory are unpredictable. Therefore, the reported temperatures are not necessarily measured at the center of an adiabatic shear band, but the thermal record certainly reflects the presence of one or more shear bands in the vicinity of the detectors.

2. RESULTS

Calibration

The response of each individual IR detector (pixel) to a given thermal signal (heated soldering iron tip) is almost identical for each pixel, when these are connected alone to the amplifier. By contrast, when all the pixels are connected simultaneously, the signal from each IR detector becomes quite different. This is due to cross-talk effects (Zehnder and Rosakis, 1991). Therefore, each channel requires an individual calibration per investigated material, with all channels connected. The calibration procedure consists of recording simultaneously the IR signal from the surface of the gauge section, along with its temperature read from a small thermocouple that is introduced at mid-thickness of the gauge (Rittel, 1999). This procedure provides a straightforward conversion of the IR detector voltage into temperature. Practically, the specimen is held in place between the bars, heated with a fan blower until it reaches the desired temperature, then allowed to cool to room temperature with the signals being recorded. Typical calibration curves of Mg AM 50 and Ti6Al4V are shown in Figure 6. Throughout this work, only 3 detectors

were used out of 8 available, to minimize cross-talk issues. IR signals from Ti6Al4V SCS specimen were observed to be much stronger than those of Mg AM50, indicating a higher emissivity of this material.

Thermo-mechanical results

Figure 7 shows typical plots of the stress and temperature as a function of strain for the 2 investigated alloys. As mentioned previously, 3 detectors are used here, and the dashed line stands for the calculated temperature rise, assuming adiabatic conditions (eqn. (2)) and a total conversion of mechanical work into heat, that is $\beta = 1$. As expected, the measured specimen's temperature increases with increasing strain. However, prior to adiabatic shear band initiation (identified as the vicinity of the decreasing stress stage), the measured temperature increase of the specimen is always lower, or at most equal to that calculated from eqn (2), assuming $\beta=1$. The measured temperature rise remains in fact quite modest, both in absolute terms and with respect to the material's melting temperature. It is only once the ASB has fully formed that a significant temperature rise is measured. Of course, at that stage the material is no longer deforming uniformly, and local strain can be very large inside the shear band. This explains the very significant measured temperature rise. The calculated temperature rise is not accurate, as a result of the localized deformation.

Marchand and Duffy (1988) used discrete visual observations of the gauge section to define threes distinct stages of ASB formation. In the present work, the same 3 stages are identified on the sole basis of thermal measurements, as follows:

Stage 1: This stage extends from $\varepsilon = 0$ to $\varepsilon\left(\sigma_{peak}\right)$. Plastic deformation is uniform, without localization, as in any other test geometry (see also (Dorogoy and Rittel, 2005)). The measured stress-strain curve represents the stress status of the entire deforming gauge section. The temperature increases quite modestly with the increasing strain. The measured temperature rise is always inferior to that calculated assuming $\beta = 1$, indicating that some of the energy is stored in the microstructure (Rittel, et al., 2006). The calculated temperature can thus be considered as an upper bound. As long as energy can be homogeneously stored into the microstructure, there appears to be no localization.

Stage 2: Spans from the strain at peak stress (or end of the plateau stress) to the strain at which the measured and calculated thermal curves intersect. During this stage, the stress is decreasing, and past the intersection point, the measured temperature exceeds the calculated limit. Referring to Marchand and Duffy (1988), the second stage can be identified as that of "heterogeneous deformation", preceding (full) localization. The deformation is not strictly homogeneous, but it is not yet fully localized. Since the measured temperature is inferior (on the average) to the calculated one, it seems that the underlying assumption of strain homogeneity is still valid to some extent to estimate the temperature rise. Strain softening at this stage is not necessarily thermal but may also indicate or result from a microstructural evolution, such as texturing or dynamic recrystallization (DRX) of part of the specimen. DRX will definitely cause local softening of the material, while being driven by mechanical strain rather than temperature (Hines and Vecchio, 1997; Perez-Prado, et al., 2001). One may also note that dynamic recrystallization is triggered by a critical level of stored energy, the latter being a constant in the system as shown in earlier work (Rittel, et al., 2006).

Stage 3: Indicates a fully formed ASB. This stage starts at the intersection point of the calculated and measured thermal curves, indicating that all of the mechanical energy transforms into heat. This point indicates the onset of the strong localization corresponding to the ASB. From here, the stress-strain curve is no longer representing the true status of the deforming gauge as a result of shear localization, and the calculated temperature rise is inaccurate. Thermal effects are indeed dominant at that stage, in the spirit of the classical models for ASB formation related to thermal softening (Zener and Hollomon, 1944).

Finally, the fracture mechanisms were characterized using scanning electron microscopy. Typical fracture surfaces are shown in Figure 8 for the two alloys. For AM50, extensive rubbing and wear of the crack faces is observed, so that the expected usual elongated micro voids are obliterated. By contrast, clear elongated dimples are observed in the fracture surface of the Ti6Al4V alloy, exactly similar to those reported by Zhou et al. (1996b). The reason for this discrepancy is not obvious at this stage, since the specimen geometries and loading conditions are essentially similar for the 2 investigated materials. One should nevertheless remark that the maximum measured homologous temperature

(for AM50 $T_{\max}/T_{melt}$=336K/708K=0.475, for Ti6Al4V $T_{\max}/T_{melt}$=445K/1877K=0.237) is much higher for the AM50 than for the Ti6Al4V alloy, so that the former is expected to locally soften more than the latter. Extensive thermal softening of the AM50 might be responsible for the quasi-total obliteration of the fracture micro-mechanisms.

3. DISCUSSION

The formation of ASB has been investigated by many researchers. However, the coupled thermo-mechanical evolution of the material for times up to and including the full development of an ASB is still not totally clear. One of the remaining open questions concerns the role of the temperature rise on the nucleation of the band. The present results offer a detailed simultaneous characterization of the stress-strain-temperature (all averaged) of the gauge section throughout the dynamic test. Marchand and Duffy (1988) divided the stress-strain curve into three stages: Homogeneous, inhomogeneous and highly localized strain, each stage being identified from the deformation of a fiducial grid pattern. The present combination of the mechanical and thermal-signals, allows a clear identification of each of these stages.

Here, one should mention the work of Liao and Duffy (1998) which is basically similar to that of Marchand and Duffy (1988) on an as-received Ti6Al4V alloy. Liao and Duffy (1998) report clear sensitivity to the initial defect geometry (Molinari and Clifton, 1987). Their results do not allow a differentiation between the stage 2 and stage 3, as the stress drops almost instantaneously, as opposed to the present results. Apart from different initial material conditions (as-received vs. annealed), the reason may be their deliberate introduction of a geometrical defect that was not introduced in the current work.

Firstly, the current results show that the temperature rise until the onset of stage 2 is relatively modest for the 2 investigated materials. During that stage (stage 1), the gauge section of the SCS deforms uniformly, as witnessed from the hardening of the stress-strain curves. Homogeneous deformation during stage 1 is identical to the homogeneous deformation of any other specimen geometry, as addressed in However, it is also interesting to consider the onset of stage 3, which marks the transition from a gradual softening to a severe localization. For the AM50 alloy, the temperature rise at the onset of stage 3 is of the order of 30K. This observation, along with the relatively small strain to

failure suggests that thermal softening, if present, is probably not the only cause of the observed softening during stage 2. Other softening mechanisms can be deemed to operate, such as dynamic recrystallization that is athermal and related to mechanical straining, as reported by Hines and Vecchio (1997). For the Ti6Al4V, the temperature rise at the onset of stage 3 is of the order of 180K, which, together with the clear observation of a stage 2, suggests that for this material, thermal softening is indeed significant. The overall influence of thermal softening is material-dependent, in the sense that strain hardening must be accounted for, and for the 2 investigated alloys, AM50 exhibits a significantly higher strain hardening that Ti6Al4V. The latter material is therefore more susceptible to thermal softening leading to and during stage 2, that AM50.

It is also interesting to note that the calculated temperature rise is indeed an upper bound, since $\beta=1$. As long as this upper bound is not exceeded, one may reasonably argue that the deformation is still sufficiently homogeneous, even if Marchand and Duffy (1988) show that it is starting to be inhomogeneous. This leads naturally to the identification of the onset of stage 3, for which the measured temperature equals, and then exceeds the calculated upper bound, indicating that the homogeneous strain assumption is violated. This clearly indicates the existence of a fully developed ASB, as observed by Marchand and Duffy (1988) on the grid pattern of their specimen.

To conclude this section, the experimental results of this work are in total agreement with those of Marchand and Duffy (1988), while tackling the problem from a different angle. The same 3 distinct stages leading to the development of an ASB until final failure are identified thermally, thus complementing the visual observations of these researchers.

4. CONCLUSIONS

- Direct monitoring of the stress-strain-temperature evolution has been achieved during dynamic testing leading to adiabatic shear failure of 2 alloys.
- Three distinct steps were identified, using thermal data, in the very spirit of Marchand and Duffy's earlier results (1988), which were obtained using visual monitoring of the gauge section.
- The stage at which an ASB is fully developed can be tentatively identified as the point at which the measured and the calculated temperature curves intersect and

diverge. This is also the strain level at which the homogeneous strain assumptions are no longer valid.

- The temperature rise of the 2 investigated alloys was found to be relatively modest until the onset of stage 2. At the onset of stage 3, it remained small for the AM50 alloy and much more significant for the Ti6Al4V.
- For AM50, thermal softening is probably not the main factor leading to ASB formation. Other factors, such as dynamic recrystallization can potentially destabilize the deformation. On the other hand, for Ti6Al4V, thermal softening appears to be more influential.

Acknowledgement: the support of the Israel Science Foundation (grant # 2002968) is gratefully acknowledged.

REFERENCES

Bai, Y., Dodd, B., 1992. Shear Localization: Occurrence, Theories, and Applications. Pergamon Press, Oxford, UK.

Boley, B.A., Weiner, J.H., 1960. Theory of Thermal Stresses. J. Wiley and Sons, New York, NY.

Dorogoy, A., 2005. personal communication.

Dorogoy, A., Rittel, D., 2005. Numerical validation of the shear compression specimen (SCS). Part I: Quasi-static large strain testing. Exp. Mech. 45 (2), 167-177.

Duffy, J., Chi, Y., 1992. On the measurement of local strain and temperature during the formation of adiabatic shear bands. Matls. Sci. Eng. A 157 (2), 195-210.

Farren, W.S., Taylor, G.I., 1925. The heat developed during plastic extension of metals. Proc. R. Soc. CVII, 422-451.

Hartley, K.A., Duffy, J., Hawley, R.H., 1987. Measurement of the temperature profile during shear band formation in mild steels deforming at high-strain rates. J. Mech. Phys. Solids 35 (3), 283-301.

Hines, J.A., Vecchio, K.S., 1997. Recrystallization kinetics within adiabatic shear bands. Acta Mater. 45 (2), 635-649

Hodowany, J., Ravichandran, G., Rosakis, A.J., Rosakis, P., 2000. Partition of plastic work into heat and stored energy in metals. Exp. Mech. 40 (2), 113-123.

Kapoor, R., Nemat-Nasser, S., 1998. Determination of temperature rise during high strain rate deformation. Mechanics of Materials 27, 1-12.

Liao, S.C., Duffy, J., 1998. Adiabatic shear band in a Ti-6Al-4V titanium alloy. J. Mech. Phys. Solids 46 (11), 2201-2231.

Macdougall, D.A.S., Harding, J., 1999. A constitutive relation and failure criterion for Ti6A14V alloy at impact rates of strain J. Mech. Phys. Solids 47 (5), 1157-1185.

Marchand, A., Duffy, J., 1988. An experimental study of the formation process of adiabatic shear bands in a structural steel. J. Mech. Phys. Solids 36 (3), 251-283.

Mason, J.J., Rosakis, A.J., Ravichandran, G., 1994. Field measurement of the dynamic deformation field around a growing adiabatic shear band at the tip of a dynamically loaded crack or notch. J. Mech. Phys. Solids 42 (11), 1679-1697.

Molinari, A., Clifton, R.J., 1987. Analytical characxterization of the shear localization in thermoviscoplastic materials J. Applied Mech. 54 (4), 806-812.

Perez-Prado, M.T., Hines, J.A., Vecchio, K.S., 2001. Microstructural evolution in adiabatic shear bands in Ta and Ta-W alloys. Acta Mater. 49, 2905-2917.

Rabin, Y., Rittel, D., 2000. Infrared temperature sensing of mechanically loaded specimens: thermal analysis. Experimental Mechanics 40 (2), 197-202.

Rittel, D., 1999. The conversion of plastic work to heat during high strain rate deformation of glassy polymers. Mechanics of Materials 31 (2), 131-139.

Rittel, D., Lee, S., Ravichandran, G., 2002. A shear compression specimen for large strain testing. Experimental Mechanics 42 (1), 58-64.

Rittel, D., Wang, Z.G., Merzer, M., 2006. Adiabatic shear failure and dynamic stored energy of cold work. Physical Review Letters 96, 075502.

Taylor, G.I., Quinney, H., 1934. The latent energy remaining in a metal after cold working. Proc. Royal Soc. London 143, 607-326.

Walley, S.M., Proud, W.G., Rae, P.J., Field, J.E., 2000. Comparison of two methods of measuring the rapid temperature rises in split Hopkinson bar specimens. Rev. Sc. Instr. 71 (4), 1766-1771.

Zehnder, A.T., Guduru, P.R., Rosakis, A.J., Ravichandran, G., 2000. Million frames per second infrared imaging system. Review of Scientific instruments 71 (10), 3762-3768.

Zehnder, A.T., Rosakis, A.J., 1991. On the tenperature distribution at the vicinity of dynamically propagating cracks in 4340 steel. J. Mech. Phys. Solids 39 (3), 385-415

Zener, C., Hollomon, J.H., 1944. Effect of strain rate upon plastic flow of steel J. Applied Phys. 15 (1), 22-32.

Zhou, M., Rosakis, A.J., Ravichandran, G., 1996a. Dynamically propagating shear bands in impact-loaded prenotched plates. II- Numerical Simulations. J. Mech. Phys. Solids 44 (6), 1007-1032.

Zhou , M., Rosakis, A.J., Ravichandran, G., 1996b. Dynamically propagating shear bands in impact-loaded prenotched plates. I- Experimental investigations of temperature signatures and propagation speed. J. Mech. Phys. Solids 44 (6), 981-1006.

Mg AM50A-F

Element	Mg	Al	Mn
Component (wt. %)	94.8-96.3	4.4-5.4	0.26-0.6

Ti6Al4V

Element	Al	Ti	V	Fe/O
Component (wt. %)	6	90	4	Max 0.2

Table I: Chemical composition of Mg AM50 and Ti6Al4V.

	Mg AM50A-F	Ti6Al4V
Density	$1.77\times10^{3}\ \mathrm{kg/m^{3}}$	$4.43\times10^{3}\ \mathrm{kg/m^{3}}$
Ultimate Tensile Strength	228 MPa	950 MPa
Tensile Yield Strength	124 MPa	880 MPa
Modulus of Elasticity	45 GPa	113.8 GPa
Poisson's Ratio	0.350	0.342
Heat capacity	1023 J/Kg-K	526 J/Kg-K

Table II: Mechanical and physical properties of Mg AM50 and Ti6Al4V.

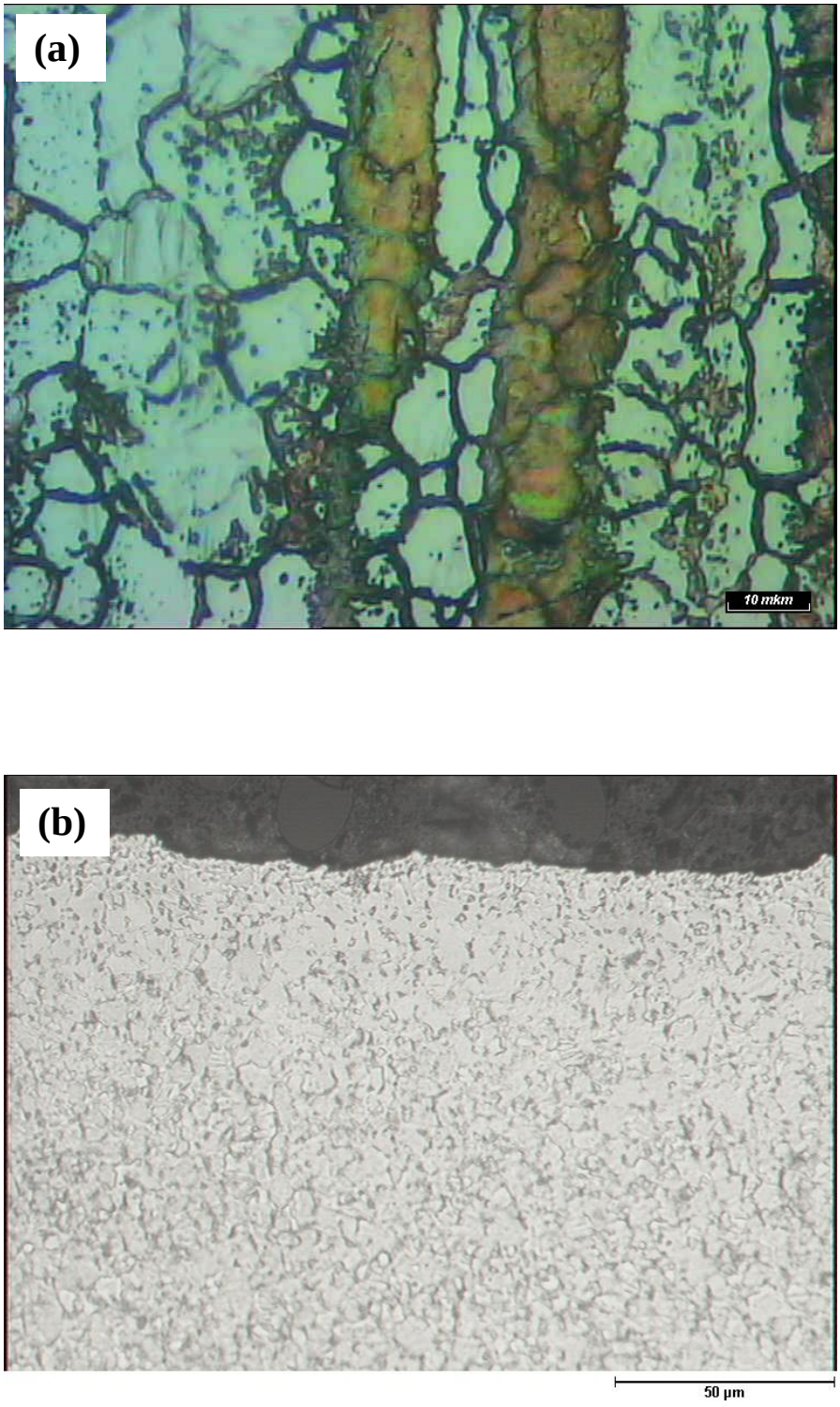

Figure 1: Typical microstructure of experimental materials: (a) AM50 and (b) Ti6Al4V.

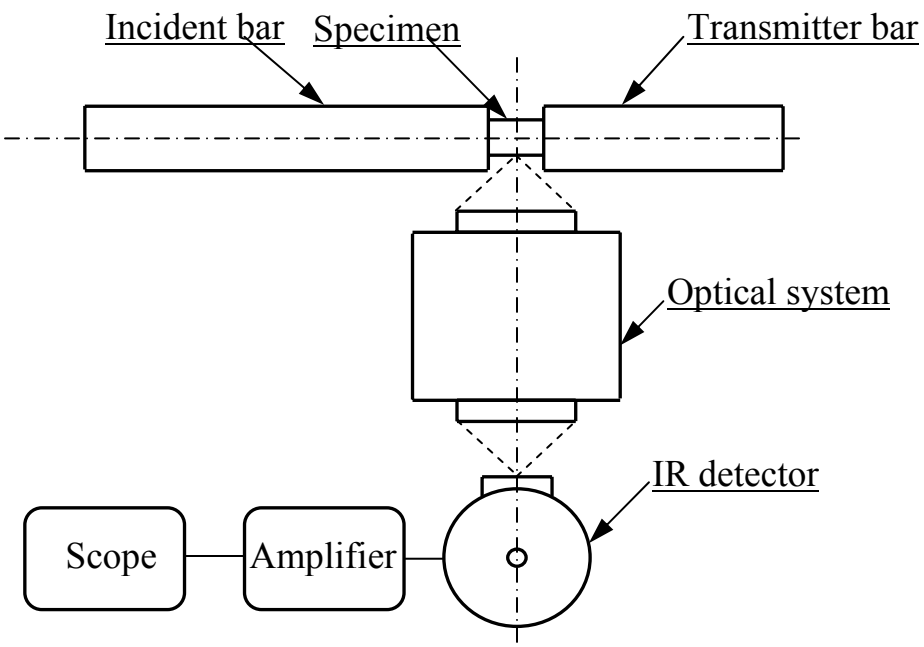

Figure 2: Schematic representations of the thermo-mechanical experimental setup.

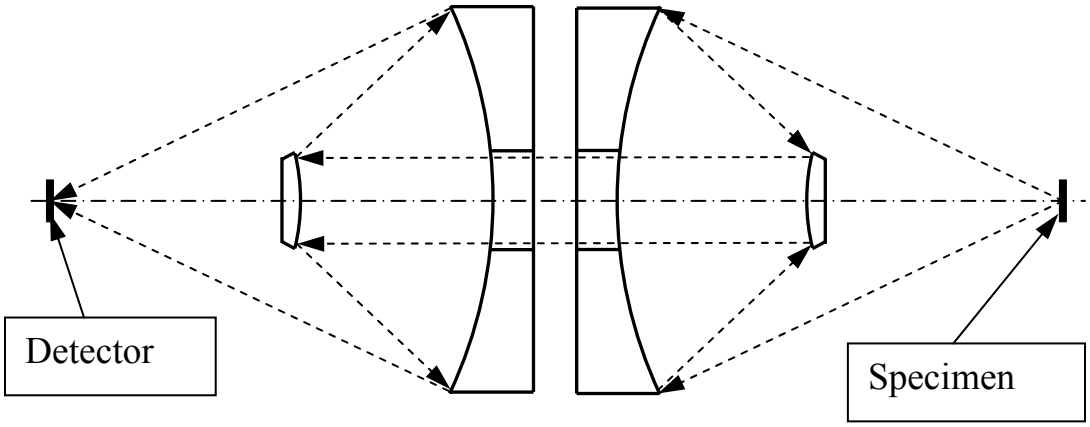

Figure 3: Schematic representation of the optical imaging system.

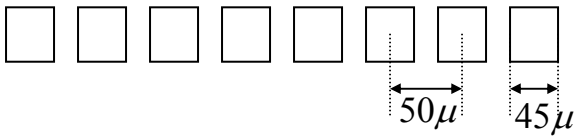

Figure 4: Layout of the pixels in the infrared detector.

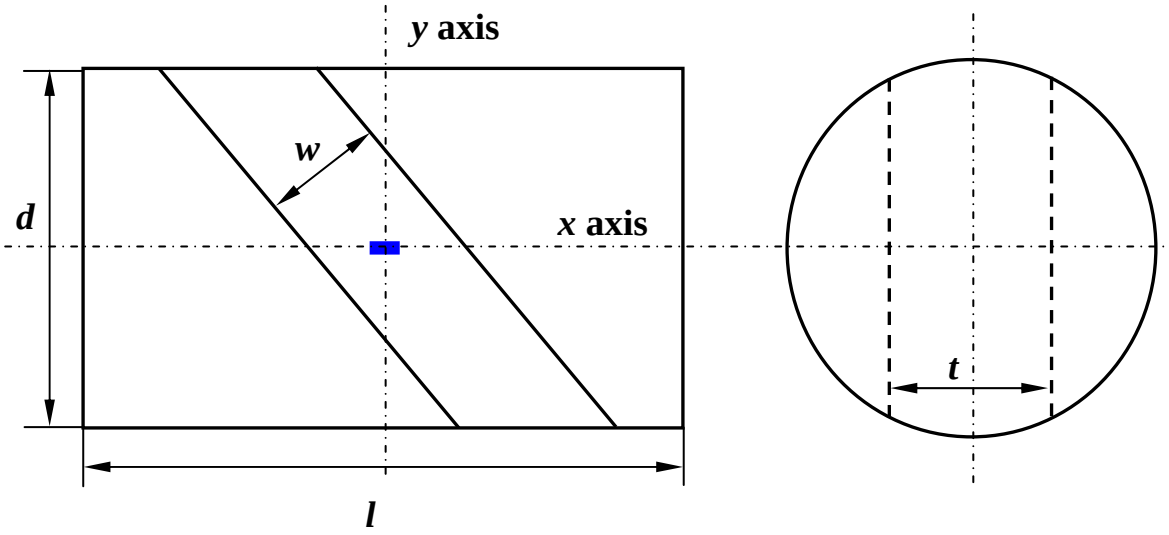

Figure 5: Focusing position of the detector on the SCS specimen (blue rectangular mark), and the dimension of the specimen: d=10mm; l=20mm; t=2.5mm; w=1.5mm (AM50), and w=2mm (Ti6Al4V)

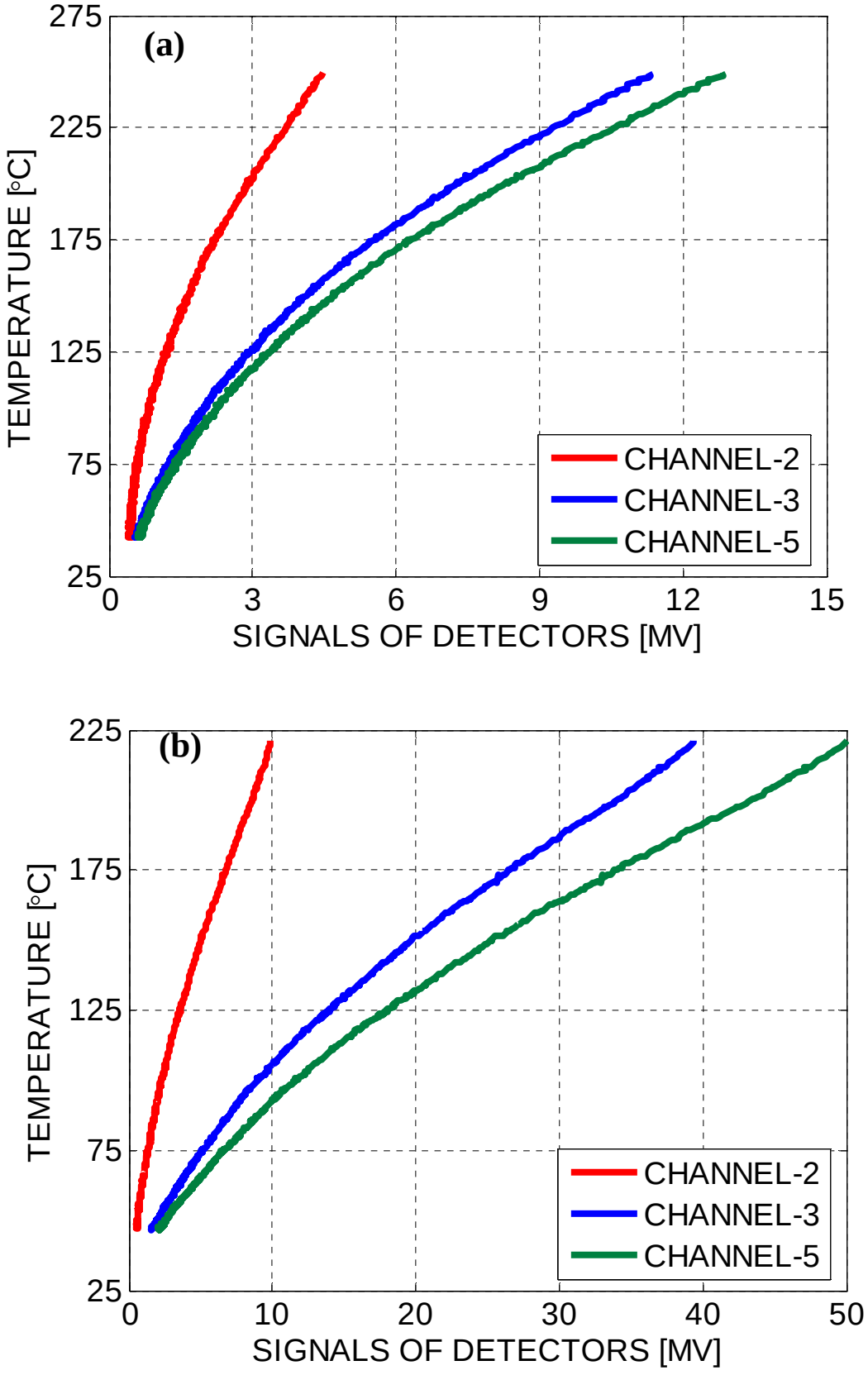

Figure 6: Typical calibration curves of (a) Mg AM50, and (b) Ti6AL4V SCS specimens

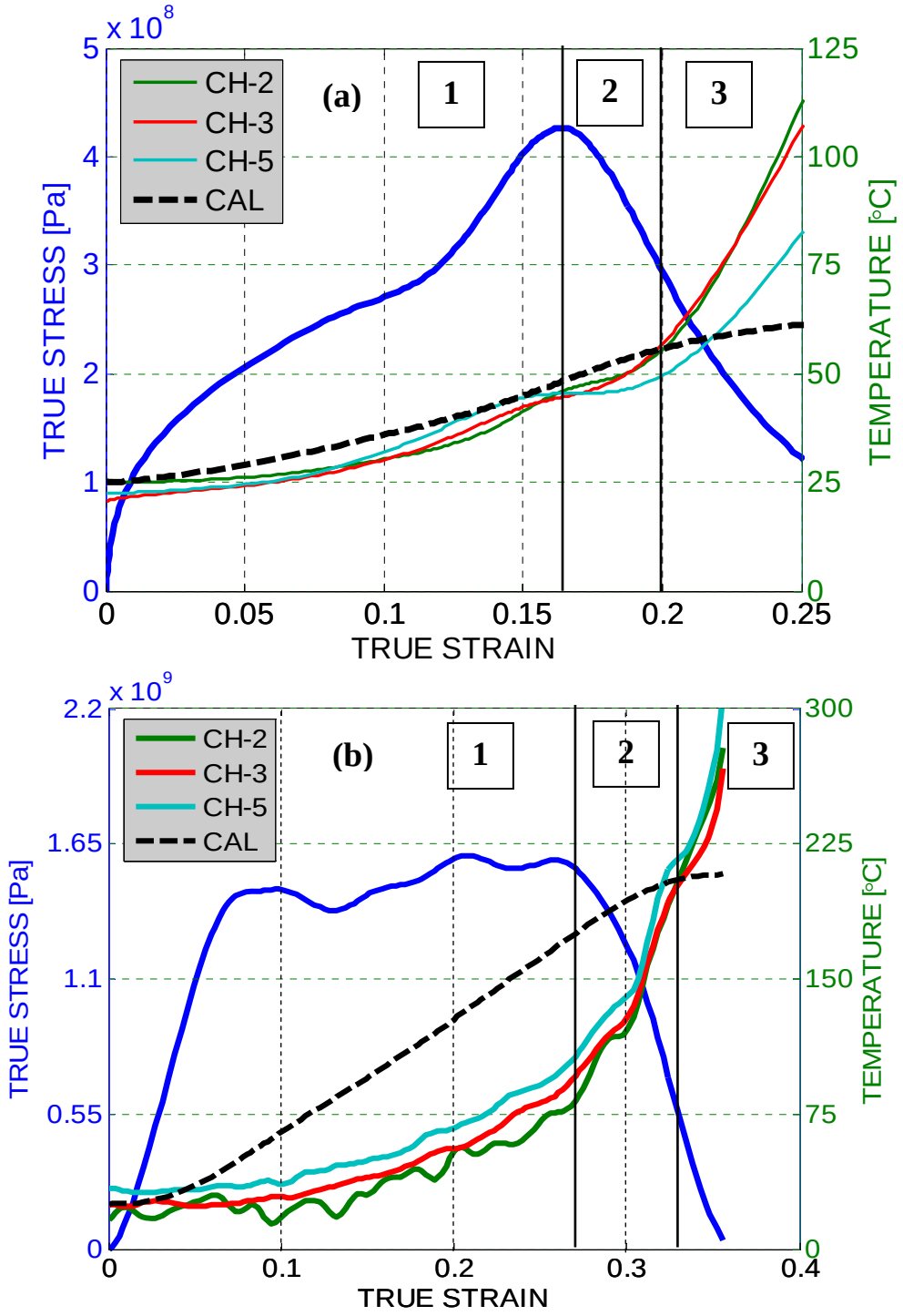

Figure 7: Typical stress and temperature vs. strain for (a) AM50 and (b) Ti6Al4V alloys. The strain rate is $\dot{\varepsilon} \approx 3000\,s^{-1}$. The temperature is measured on 3 channels and calculated (dashed line) according to β=1. Three stages are indicated: stage 1 where the deformation proceeds homogeneously and the temperature rise is quite modest, stage 2 with a heterogeneous deformation, where the measured temperature is still inferior to the (upper bound) calculated, and stage 3, starting at the intersection point between the thermal curves. For this stage, the ASB is fully developed and the calculated homogeneous temperature rise is inaccurate.

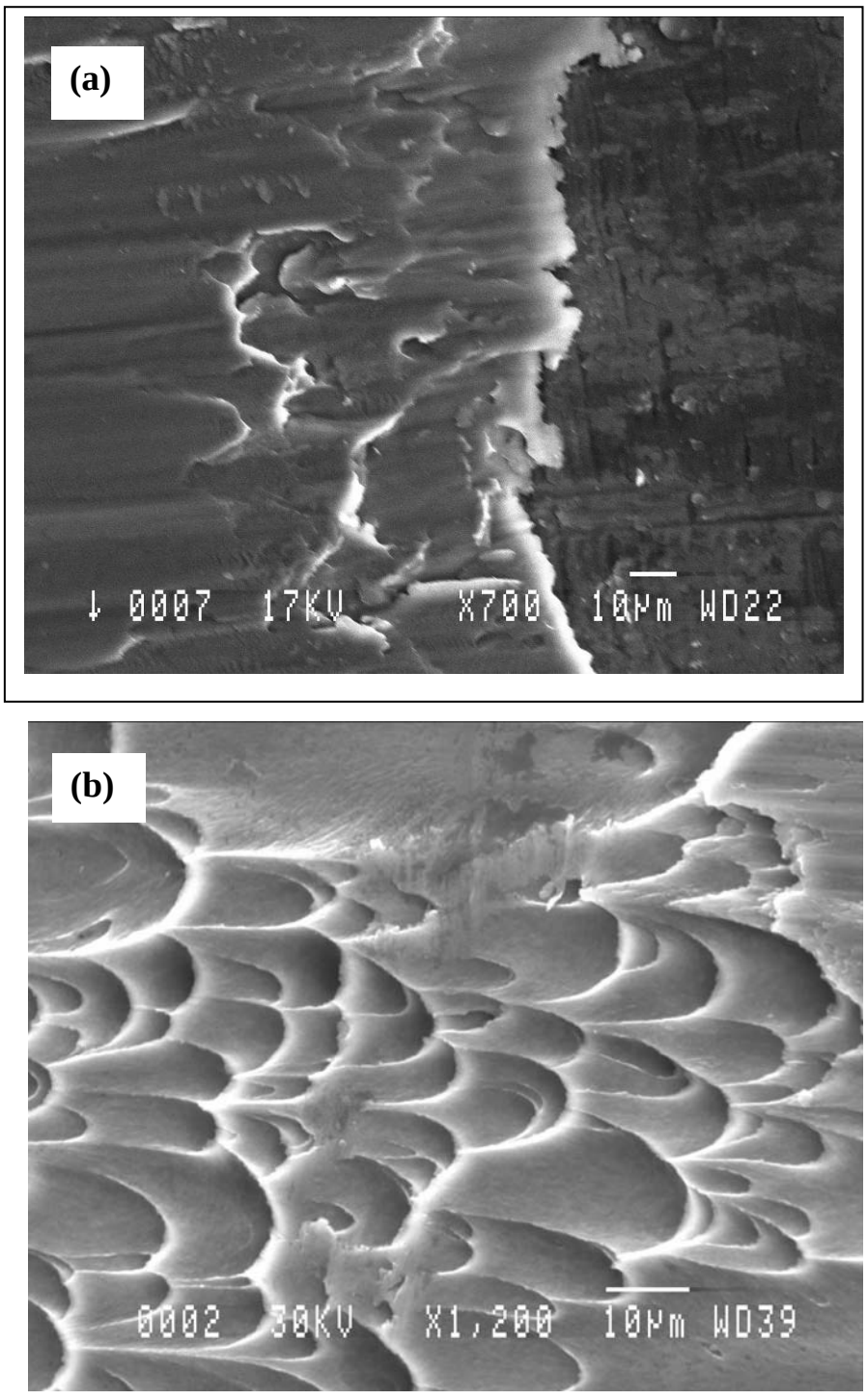

Figure 8: Fracture surface topography of (a) AM50 and (b) Ti6Al4V. While the topography of (a) shows extensive wear, elongated dimples are clearly discernable in (b). One reason for extensive wear of AM50 may be the high homologous temperature reached locally at failure.